

Equilibrium, metastability, and hysteresis in a model spin-crossover material with nearest-neighbor antiferromagnetic-like and long-range ferromagnetic-like interactions

Per Arne Rikvold,¹ Gregory Brown,² Seiji Miyashita,^{3,4} Conor Omand,^{3,5} and Masamichi Nishino⁶

¹*Department of Physics, Florida State University, Tallahassee, Florida 32306-4350, USA*

²*Computational Science and Mathematics Division, Oak Ridge National Laboratory, Oak Ridge, Tennessee 37830, USA*

³*Department of Physics, Graduate School of Science, The University of Tokyo, 7-3-1 Hongo, Bunkyo-ku, Tokyo 113-8656, Japan*

⁴*CREST, JST, 4-1-8 Honcho Kawaguchi, Saitama, 332-0012, Japan*

⁵*Department of Physics and Astronomy, University of British Columbia, Vancouver, BC, Canada V6T 1Z4*

⁶*Computational Materials Science Center, National Institute for Materials Science, Tsukuba, Ibaraki 305-0047, Japan*

(Received 21 October 2015; revised manuscript received 27 January 2016; published 16 February 2016)

Phase diagrams and hysteresis loops were obtained by Monte Carlo simulations and a mean-field method for a simplified model of a spin-crossover material with a two-step transition between the high-spin and low-spin states. This model is a mapping onto a square-lattice $S = 1/2$ Ising model with antiferromagnetic nearest-neighbor and ferromagnetic Husimi-Temperley (equivalent-neighbor) long-range interactions. Phase diagrams obtained by the two methods for weak and strong long-range interactions are found to be similar. However, for intermediate-strength long-range interactions, the Monte Carlo simulations show that tricritical points decompose into pairs of critical end points and mean-field critical points surrounded by horn-shaped regions of metastability. Hysteresis loops along paths traversing the horn regions are strongly reminiscent of thermal two-step transition loops with hysteresis, recently observed experimentally in several spin-crossover materials. We believe analogous phenomena should be observable in experiments and simulations for many systems that exhibit competition between local antiferromagnetic-like interactions and long-range ferromagnetic-like interactions caused by elastic distortions.

DOI: [10.1103/PhysRevB.93.064109](https://doi.org/10.1103/PhysRevB.93.064109)

I. INTRODUCTION

In many materials, local elastic interactions induce effective long-range interactions via the macroscopic strain field [1,2]. In addition to elastic crystals, physical realizations of long-range interactions include systems as diverse as earthquake faults [3] and long-chain polymers [4]. Phase transitions in such systems belong to the *mean-field universality class*, which has some unusual properties. In particular, critical clusters can be strongly suppressed compared to transitions caused by purely short-range interactions. This effect should be experimentally observable as an absence of critical opalescence [5–7].

A particular class of systems that exemplify these interesting properties are *spin-crossover* (SC) materials [5–12]. These are molecular crystals in which the individual organic molecules contain transition metal ions, such as Fe(II), Fe(III), or Co(II), that can exist in two different spin states: a low-spin ground state (LS) and a high-spin excited state (HS). Molecules in the HS state have higher effective degeneracy and larger volume than those in the LS state. Due to the higher degeneracy of the excited HS state, crystals of such molecules can be brought into a majority HS state by increasing temperature, changing pressure or magnetic field, or by exposure to light [8,13–17]. If the intermolecular interactions are sufficiently strong, this change of state can become a discontinuous phase transition such that the HS phase becomes metastable and hysteresis occurs [13,18]. In the case of optical excitation into the metastable phase, this effect is known as light-induced excited spin-state trapping (LIESST) [13,19]. The different magnetic and optical properties of the two phases make such cooperative SC materials promising candidates for applications such as switches, displays, memory devices, sensors, and activators [15,17,20,21].

Various experimental results over the past decade have led to the suggestion that the dominant interaction mechanism in SC materials is elastic and therefore effectively long range, due to the larger size of the molecule in its HS state [9,22]. Such systems can be modeled by a pseudospin Hamiltonian of the form

$$\mathcal{H} = -J \sum_{(i,j)} s_i s_j - \frac{1}{2} (k_B T \ln g - D) \sum_i s_i + \mathcal{H}_{\text{LR}}. \quad (1)$$

The first two terms constitute the Wajnflasz-Pick Ising-like model [23], in which the pseudospin variables s_i denote the two spin states (-1 for LS and $+1$ for HS), and J is a nearest-neighbor interaction. The effective field term,

$$H = (k_B T \ln g - D)/2, \quad (2)$$

contains $D > 0$, which is the energy difference between the HS and LS states, g , which is the ratio between the HS and LS degeneracies, and $k_B T$, the absolute temperature in energy units. The long-range interactions are represented by \mathcal{H}_{LR} . The usual order parameter for SC materials is the proportion of HS molecules, n_{HS} , which is related to the pseudospin variables as $n_{\text{HS}} = (m + 1)/2$, where $m = \sum_i s_i / N$ (with N the total number of molecules) is the pseudomagnetization.

While the long-range term \mathcal{H}_{LR} is most often considered as a true elastic interaction [5,7,24], many aspects of the model can be obtained at much lower computational cost by replacing this by a Husimi-Temperley (also known as equivalent-neighbor) effective Hamiltonian [6,25]. The latter is the approach we follow in the present paper.

In previous work we have considered models of SC materials that show a direct, or one-step, transition between the LS and HS phases. In these cases, the short-range interactions

favor configurations in which nearest-neighbor molecules are in the same state (LS-LS or HS-HS). This corresponds to a positive short-range interaction constant J in Eq. (1). In the pseudospin language often used in the SC literature, this case is called ferromagnetic-like, or simply ferromagnetic. We emphasize that this is only an analogy and does *not* imply a magnetic character of the interactions. In the remainder of this paper, we will use the simplified terms, ferromagnetic and antiferromagnetic, for interactions that favor uniform and checkerboard spin-state arrangements, respectively.

When both the short-range and long-range interactions are ferromagnetic, any nonzero long-range interaction has the effect of changing the universality class of the critical point of the LS/HS phase transition caused by the short-range interactions from the Ising to the mean-field universality class [6]. As a result, critical clusters are suppressed, and the system develops true metastable phases limited by sharp spinodal lines in the phase diagram.

There also exist SC materials, in which the transition between the LS and HS phases proceeds as a two-step transition via an intermediate phase [26–40]. For some materials, such as Fe(II)[2-picolyamine]₃Cl₂ · ethanol [26], it has been shown by x-ray diffraction that spontaneous symmetry breaking induces an intermediate phase, characterized by long-range order on two interpenetrating sublattices with nearest-neighbor molecules in different states (HS-LS) [41,42]. This situation can be modeled by the Ising-like model of Eq. (1) with antiferromagnetic nearest-neighbor interactions ($J < 0$). Various mean-field approximations to this model have been considered, both with [27,29,34] and without [33] a long-range ferromagnetic term.

In a recent work, Nishino and Miyashita studied such a model using an elastic long-range interaction [24]. They found that, for weak applied field, the antiferromagnetic phase transition remains in the Ising universality class. At low temperatures they observed tricritical points separating lines of second-order and first-order phase transitions. However, much of their high-temperature analysis replaced the short-range interactions by a two-sublattice mean-field model, which neglects the effects of local fluctuations. The aim of the present paper is to investigate the effects of such fluctuations in an Ising-like model with nearest-neighbor antiferromagnetic interactions and a long-range ferromagnetic interaction of the Husimi-Temperley form. This enables us to obtain excellent long-time statistics for systems with over one million individual pseudospins, and for several different values of the long-range interaction strength. Some preliminary results were included in Ref. [43].

The organization of the rest of the paper is as follows. In Sec. II we present the Ising Hamiltonian with antiferromagnetic nearest-neighbor interactions and a ferromagnetic Husimi-Temperley type long-range interaction of adjustable strength. Here we also obtain ground-state diagrams (zero-temperature phase diagrams) including phase coexistence points and spinodal points for different strengths of the long-range interaction term. In Sec. III we present results for a mean-field approximation to this model, in which the nearest-neighbor antiferromagnetic interactions are replaced by a two-sublattice mean-field approximation. Two different strengths of the long-range ferromagnetic interactions, which

yield qualitatively different phase diagrams, are considered. In Sec. IV we return to our original, nearest-neighbor antiferromagnetic interactions, investigating the resulting phase diagrams by Metropolis importance-sampling Monte Carlo (MC) simulations. We find that, in a certain range of the long-range interaction strength, the resulting phase diagrams are qualitatively different from those obtained by the mean-field approximations. In particular, tricritical points predicted by the mean-field approximations are found by MC to decompose into pairs of critical end points and mean-field critical points surrounded by horn-shaped regions of metastability. Here we also present hysteresis curves that are particularly relevant to the system's interpretation as a model of two-step transitions in SC materials. Our conclusions and suggestions for future work are presented in Sec. V.

II. HAMILTONIAN AND GROUND-STATE ANALYSIS

The square-lattice Ising antiferromagnet with weak, long-range (Husimi-Temperley) ferromagnetic interactions is defined by the Hamiltonian

$$\mathcal{H} = -J \sum_{(i,j)} s_i s_j - N \left(H + \frac{A}{2} m \right) m, \quad (3)$$

with $J < 0$ and $A > 0$. Here, H is the applied field, $s_i = \pm 1$, and $m = N^{-1} \sum_i s_i$. For a square lattice of side L , $N = L^2$. The strength of the long-range interaction is A . It is defined such that the critical temperature of the pure long-range ferromagnet ($J = 0$) equals A/k_B , where k_B is Boltzmann's constant. For convenience we will hereafter use the dimensionless variables, $h = H/|J|$, $a = A/|J|$, and $t = k_B T/|J|$.

The model's equilibrium and metastable phases at zero temperature are found by a simple ground-state analysis. The per-site energies of the fully ordered antiferromagnetic (AFM) and field-induced ferromagnetic (FM) phases are given by $E_{\text{AFM}}/(N|J|) = -2$, $E_{+}/(N|J|) = 2 - a/2 - h$, and $E_{-}/(N|J|) = 2 - a/2 + h$, respectively. Equating the AFM and FM energies yields the zero-temperature transition values of h as

$$h_{\text{AFM}/+} = 4 - a/2 \quad (4)$$

and

$$h_{\text{AFM}/-} = -4 + a/2. \quad (5)$$

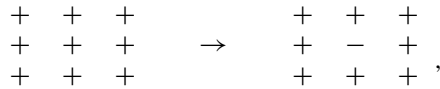
For $a > 8$, the AFM ground state disappears, and the system in equilibrium has a direct transition between the $m = -1$ and $m = +1$ FM ground states at $h = 0$. (For $a = 8$, the AFM and both FM ground states are degenerate at $h = 0$.)

The limits of local stability of metastable phases at $t = 0$ (zero-temperature spinodal fields) are the field values at which the energy change due to a flip of a single spin in the metastable phase becomes negative [44]. For metastability, a positive energy change is required. The spinodal fields are determined as follows.

A. $a < 8$

Decreasing h , attempting to nucleate a transition from metastable $m = +1$ to the AFM or $m = -1$ ground state by a

single spin flip,

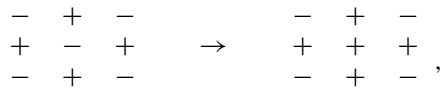


the energy change is

$$\begin{aligned} \Delta E/|J| &= -8 + 2h + 2a(1 - 1/N) > 0 \\ &\Rightarrow h > 4 - a(1 - 1/N). \end{aligned} \quad (6)$$

Thus (in the limit $N \rightarrow \infty$) the $m = +1$ phase is metastable for $4 - a < h < 4 - a/2$. By symmetry, the $m = -1$ phase is metastable for $-4 + a/2 < h < -4 + a$.

Increasing h , attempting to nucleate a transition from metastable AFM to the $m = +1$ ground state by a single spin flip,



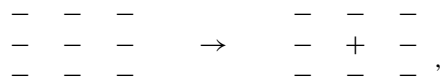
the energy change is

$$\Delta E/|J| = 8 - 2h - 2a/N > 0 \Rightarrow h < 4 - a/N. \quad (7)$$

Thus (in the limit $N \rightarrow \infty$) the AFM phase is metastable against decay to $m = +1$ for $4 - a/2 < h < 4$. By symmetry, the AFM phase is metastable against decay to $m = -1$ for $-4 < h < -4 + a/2$. Four mean-field sharp spinodal lines extend from these zero-temperature spinodal points toward higher t . The zero-temperature limits of the phase diagrams shown in Figs. 1(a), 4(a), and 5(a) illustrate the positions of coexistence and spinodal points for values of $a < 8$.

B. $a > 8$

The only ground states are $m = +1$ for $h \geq 0$ and $m = -1$ for $h \leq 0$. Increasing h , attempting to nucleate a transition from metastable $m = -1$ to the $m = +1$ ground state by a single spin flip,



the energy change is

$$\begin{aligned} \Delta E/|J| &= -8 - 2h + 2a(1 - 1/N) > 0 \\ &\Rightarrow h < a(1 - 1/N) - 4. \end{aligned} \quad (8)$$

Thus (in the limit $N \rightarrow \infty$) $m = -1$ is metastable for $0 < h < a - 4$. By symmetry, $m = +1$ is metastable for $-a + 4 < h < 0$. Using Eq. (7) and symmetry, we find that the AFM state, while never a ground state, is metastable for $-4 < h < 4$. The zero-temperature limits of the phase diagrams shown in Figs. 3(a) and 9(a) illustrate the positions of coexistence and spinodal points for $a > 8$.

III. MEAN-FIELD APPROXIMATION

In order to obtain an approximate picture of the behavior of the model at finite t , we employ a simple, two-sublattice Bragg-

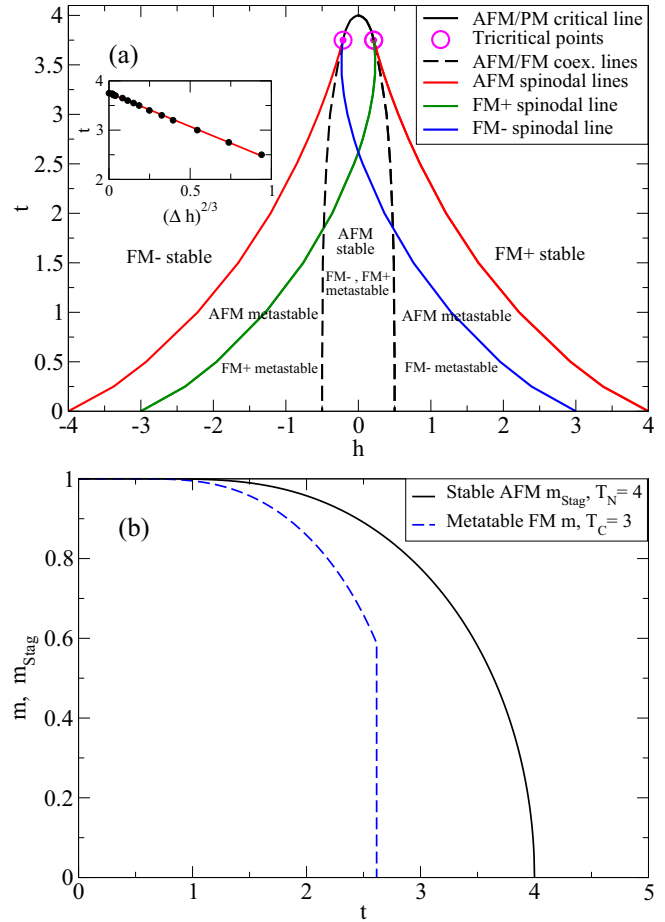


FIG. 1. Mean-field phase diagrams for $a = 7 < 8$. (a) In the h, t plane, showing a line of equilibrium critical points terminated by two tricritical points, equilibrium coexistence lines, and sharp spinodals. The FM+ phase is stable everywhere on the positive- h side of the right-hand coexistence line, and analogously for FM- on the negative- h side. The inset demonstrates the $(t_c - t)^{3/2}$ behavior of the spinodal fields, as given by Eq. (15). Here, Δh is the difference between the FM and corresponding AFM spinodals. (b) Showing the stable AFM order parameter m_{Stag} and the metastable FM order parameter m vs t for $h = 0$. The latter terminates at the spinodal temperature $t_{\text{sFM}} \approx 2.615$, corresponding to the crossing of the two FM spinodal field curves in part (a). See further discussion in the text.

Williams mean-field approximation [27,29,33,45,46] with sublattice magnetizations $m_A = 2N^{-1} \sum_{i \in A} s_i$ on sublattice A ($m_A \in [-1, +1]$) and analogously for m_B on sublattice B. The magnetization and staggered magnetization are given by $m = (m_A + m_B)/2$ and $m_{\text{Stag}} = (m_A - m_B)/2$, respectively. The approximation is defined by the Hamiltonian

$$\begin{aligned} \frac{\mathcal{H}_{\text{MFA}}}{N|J|} &= \frac{4}{2} m_A m_B - \frac{a}{2} m^2 - h m = \frac{1}{2} \left(4 - \frac{a}{2} \right) m_A m_B \\ &\quad - \frac{a}{8} (m_A^2 + m_B^2) - \frac{h}{2} (m_A + m_B). \end{aligned} \quad (9)$$

Note that the effective interaction between the two sublattice magnetizations includes the long-range interaction strength a and changes sign from AFM for weak a to FM for strong a

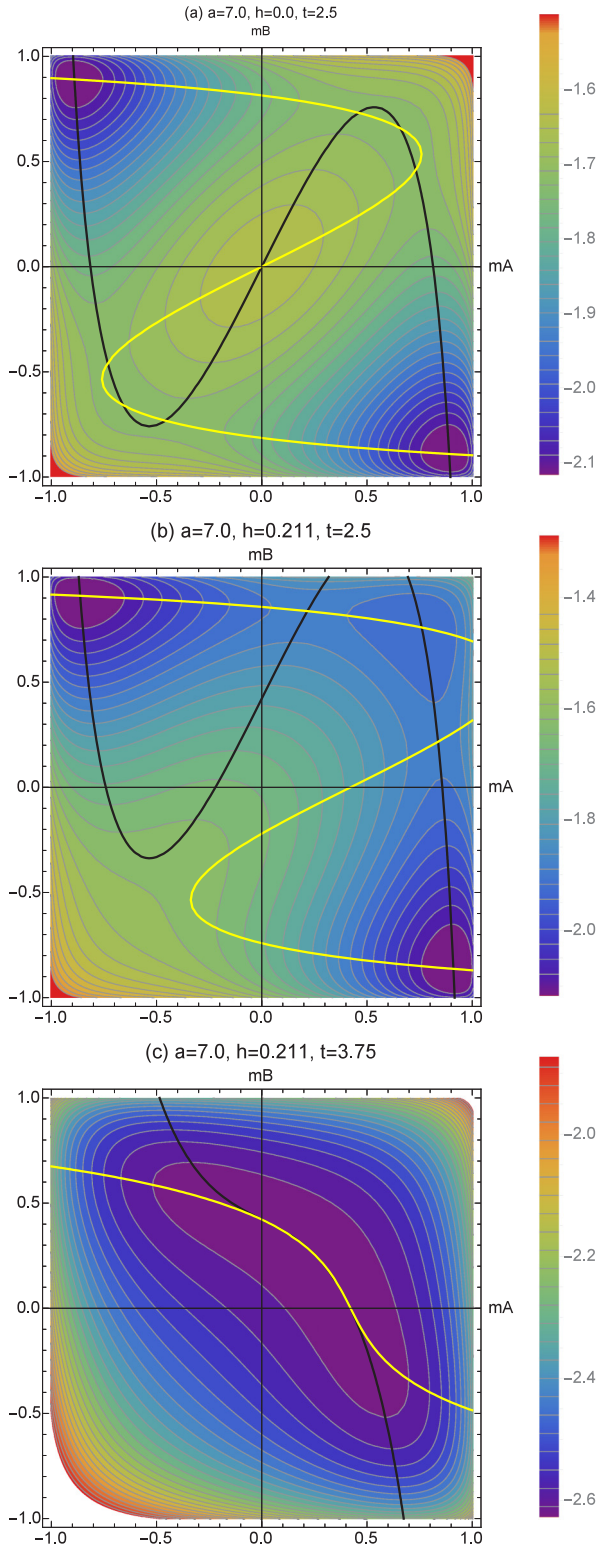


FIG. 2. Contour plots in the m_A, m_B plane of the mean-field free energy for $a = 7$. The black and light gray (yellow online) curves represent the solutions of $\partial F_{\text{MFA}}/\partial m_A = 0$ and $\partial F_{\text{MFA}}/\partial m_B = 0$, respectively. Crossings of the curves correspond to extrema and saddle points of the free-energy surfaces. (a) $t = 2.5$ and $h = 0$. Global minima in the second and fourth quadrant represent the degenerate AFM stable phases. Local minima in the first and third quadrants represent the degenerate FM metastable phases. (b) $t = 2.5$ and $h = 0.211$. Global minima in the second and fourth quadrants

at $a = 8$. For $a = 8$, the mean-field approximation describes two independent, ferromagnetic sublattices.

The system entropy in the mean-field approximation is the sum of the two sublattice entropies,

$$S_{\text{MFA}} = -\frac{N}{2} \sum_{X=A}^B \left(\frac{1+m_X}{2} \ln \frac{1+m_X}{2} + \frac{1-m_X}{2} \ln \frac{1-m_X}{2} \right), \quad (10)$$

and the resulting free energy is [45–47]

$$F_{\text{MFA}} = \mathcal{H}_{\text{MFA}} - k_B T S_{\text{MFA}}. \quad (11)$$

The coupled self-consistency equations, $\partial F_{\text{MFA}}/\partial m_A = 0$ and $\partial F_{\text{MFA}}/\partial m_B = 0$, become

$$m_A = \tanh \left[\frac{\left(\frac{a}{2} - 4\right)m_B + \frac{a}{2}m_A + h}{t} \right] \quad (12)$$

and equivalent for m_B with A and B interchanged on the right-hand side.

For $a < 8$ and $h = 0$, the global free-energy minima lie along the AFM axis ($m_B = -m_A$) in the order-parameter plane, and the self-consistency equation for the staggered magnetization becomes

$$m_{\text{stag}} = \tanh \frac{4m_{\text{stag}}}{t}, \quad (13)$$

with the Néel temperature $t_N = 4$, independent of a . For $a > 8$ and $h = 0$, the global free-energy minima lie along the FM axis ($m_B = m_A$), and the self-consistency equation for the magnetization becomes

$$m = \tanh \frac{(a-4)m}{t}, \quad (14)$$

with the a -dependent Curie-Weiss critical temperature $t_C = (a-4)$. For nonzero applied fields, free-energy minima and saddle points in the (m_A, m_B) plane were obtained numerically using Mathematica. Resulting phase diagrams for $a = 7$ and $a = 10$ are shown in Figs. 1 and 3, respectively.

A. $a = 7$

Typical mean-field phase diagrams for the model with $a < 8$ are shown in Fig. 1, here using $a = 7$. In Fig. 1(a), the line of Néel critical points, marking the continuous phase transition between the stable AFM phase and the high-temperature disordered phase, extends from $t_N = 4$ to two tricritical points at a lower temperature, which decreases with decreasing a . [For $a = 7$, the tricritical points are found at $t_3 \approx 3.75$ and $h_3 \approx \pm 0.211$, as seen in Figs. 1(a) and 2(c).] Lines of first-order phase transitions (AFM/FM coexistence lines) extend from the tricritical points to the zero-temperature coexistence points at $h = \pm(4 - a/2) = \pm 0.5$. Sharp spinodal field lines marking

represent the degenerate AFM stable phases. The local minimum in the first quadrant represents the metastable FM+ phase. (c) $t = 3.75$ and $h = 0.211$, corresponding to the tricritical point where the two AFM and the FM+ phases are indistinguishable. The shallow, global minimum lies in the first quadrant along the FM ($m_B = m_A$) axis.

the limits of metastability for the AFM phase extend from the tricritical points to the zero-temperature spinodal points at $h = \pm 4$, and spinodals marking the limits of metastability for the FM+ and FM- phases extend to their zero-temperature termination points at $h = 4 - a = -3$ and $h = -4 + a = +3$, respectively. The corresponding zero-field order parameters, the equilibrium AFM m_{Stag} and the metastable FM m , which follow Eqs. (13) and (14), respectively, are shown in Fig. 1(b). However, the free-energy barriers that prevent the decay of the metastable FM phases (which are possible at $h = 0$ only for $4 < a < 8$) into an AFM phase vanish at a spinodal temperature $t_{\text{sFM}} \approx 2.615$, marked by a discontinuous drop of m to zero. This temperature corresponds to the crossing of the two FM spinodals in Fig. 1(a). Above it, the FM solutions of the self-consistency equations become saddle points. Samples of free-energy contour plots in the m_A, m_B plane, based on Eq. (11), overlaid with curves representing the individual solutions of the two self-consistency equations, Eq. (12), are shown in Fig. 2.

Mean-field models of two-step crossover have previously been considered by Zelentsov *et al.* [27], Bousseksou *et al.* [29], and Bolvin [33], with Bragg-Williams approaches similar to ours, and by Chernyshov *et al.* [34] using Landau theory. However, Bolvin does not include any FM interaction, and consequently the resulting mean-field phase diagrams are those of a pure Ising antiferromagnet without any first-order transitions (Figs. 5 and 6 of Ref. [33]). Zelentsov *et al.* and Bousseksou *et al.* confine the FM interactions to each sublattice separately, and so these interactions do not affect the effective intersublattice interaction as they do in our model [see Eq. (9)]. Neither paper contains explicit phase diagrams. However, their plots of HS fraction versus temperature indicate that phase diagrams for the case of identical sublattices (their intrasublattice interactions $J_A = J_B$) should be similar to ours, including tricritical points and first-order transitions at low temperatures. However, their intrasublattice FM interactions lower the energies of the FM and AFM ground states by the same amount, with the result that they, in contrast to the corresponding term in our model, do not influence the ground-state diagram of the pseudospin model. In that respect, their approaches would correspond to a mean-field approximation to a square-lattice Ising model with AFM nearest-neighbor (intersublattice) and FM next-nearest neighbor (intrasublattice) interactions [48–50]. In the Landau-theory approach of Chernyshov *et al.*, the ferromagnetic interactions are not limited to the separate sublattices. For not too negative values of their temperature-like parameter α_2 , the phase diagram in Fig. 5 of Ref. [34] is quite similar to our Fig. 1(a). We believe an approach in which the ferromagnetic interactions are not limited to the individual sublattices provides a better approximation for the effects of a long-range elastic interaction.

B. $a = 10$

Figure 3 shows typical mean-field phase diagrams for the model with $a > 8$, here using $a = 10$. There are only FM equilibrium phases, which coexist at $h = 0$ up to the Curie temperature, $t_c = a - 4 = 6$. In Fig. 3(a), sharp spinodal field lines marking the limits of metastability for the FM+ and FM-

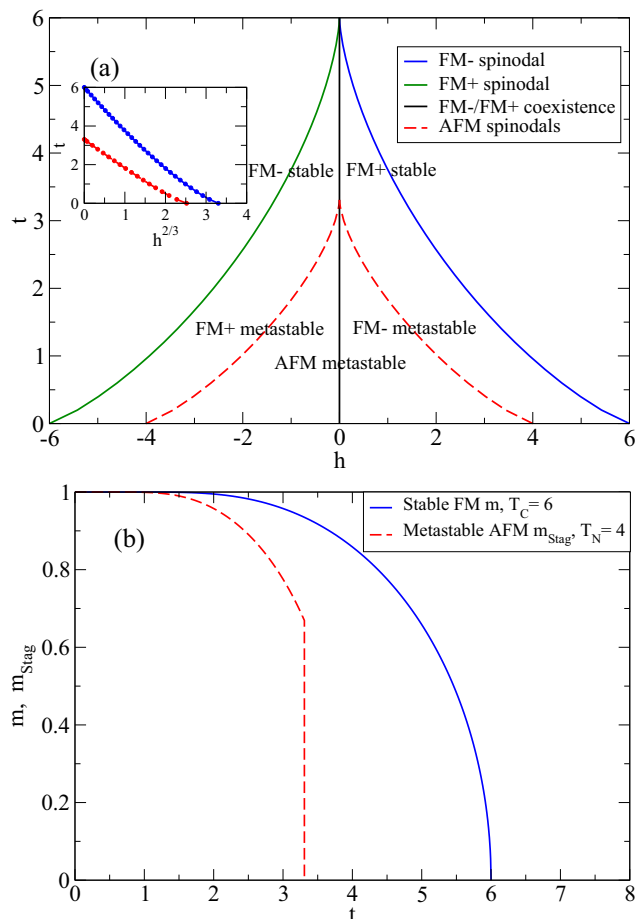


FIG. 3. Mean-field phase diagrams for $a = 10 > 8$. (a) In the h, t plane, showing the equilibrium coexistence line at $h = 0$ and the spinodal field curves. The inset demonstrates the $(t_c - t)^{3/2}$ behavior of the spinodal fields, as given by Eq. (15). (b) Showing the stable FM order parameter m and the metastable AFM order parameter m_{Stag} vs t at $h = 0$. The latter terminates at the spinodal temperature $t_{\text{sAFM}} \approx 3.308$, corresponding to the meeting of the two AFM spinodal field curves in part (a). See further discussion in the text.

phases extend from the critical point to their zero-temperature termination points at $h = 4 - 10 = -6$ and $h = -4 + 10 = +6$, respectively. Two degenerate, metastable AFM phases are possible at low t and h , and the spinodals marking their limits of local stability are also shown. The corresponding zero-field order parameters, the equilibrium FM m and the metastable AFM m_{Stag} , which follow Eqs. (14) and (13), respectively, are shown in Fig. 3(b). However, the metastable AFM phases become unstable toward decay into a FM phase at a spinodal temperature $t_{\text{sAFM}} \approx 3.308$, where the two AFM spinodals meet in Fig. 3(a).

In both ranges of the long-range interaction strength a , near the critical, tricritical, or spinodal temperature the spinodal fields obey the power law [51],

$$|h_{\text{Spin}} - h_{\text{Coex}}| \sim (t_c - t)^{3/2}, \quad (15)$$

where h_{Spin} and h_{Coex} are the spinodal and coexistence fields, respectively, and t_c represents the appropriate temperature where they meet. This is shown in the insets in Figs. 1(a) and 3(a).

IV. MONTE CARLO SIMULATIONS

The standard mean-field approximation for the short-range interactions, discussed in Sec. III, does not properly describe the microscopic fluctuations that are important in low-dimensional systems, especially near critical and multicritical points [52,53]. We therefore return to the full model described by Eq. (3) to further investigate its phase diagrams and dynamics using importance-sampling Metropolis MC simulations. We consider $L \times L$ square lattices with $L = 64, \dots, 1024$ and periodic boundary conditions. Results are extrapolated to the thermodynamic limit using known finite-size scaling relations.

Critical points are located by crossings of fourth-order Binder cumulants [54] for the antiferromagnetic order parameter m_{Stag} ,

$$U_L = 1 - \frac{\langle m_{\text{Stag}}^4 \rangle_L}{3 \langle m_{\text{Stag}}^2 \rangle_L^2}. \quad (16)$$

(In general, the moments included in this equation are *central moments*, but since the model contains no staggered field, this is automatically satisfied for the moments of m_{Stag} .) This method significantly reduces finite-size effects, and the results are further linearly extrapolated to $1/L = 0$ [6]. For isotropic interactions and periodic boundary conditions on a square lattice, as used here, the Ising fixed-point value of the cumulant is $U^* = 0.61 \dots$ [55–57].

Coexistence lines represent first-order phase transitions between stable equilibrium phases, i.e., equality of the corresponding bulk free energies. Here, we locate the coexistence lines by starting simulations from an initial configuration consisting of two slabs, one in the AFM ground state and one in the FM ground state corresponding to the sign of h (mixed start method), and searching for the field at which the final state would be either with approximately 50% probability.

The long-range, ferromagnetic interactions produce a finite barrier in the free-energy *density*, separating the metastable and stable phases. As a result, the *total* free-energy barrier increases linearly with the system size, $N = L^2$, leading to an exponential size divergence for the lifetime of such a “true” metastable phase [25,58]. (We note that this situation is radically different from the case of metastable decay in systems with only local interactions. In that case, the decay occurs through nucleation and growth of compact droplets of the stable phase, and the metastable lifetime becomes system-size *independent* in the thermodynamic limit [59].) The sharp spinodal lines at which the free-energy barrier vanishes are located by starting an $L \times L$ system in the equilibrium phase and slowly scanning h past the coexistence line (where the initial phase becomes metastable) until the order parameters undergo simultaneous, discontinuous jumps denoting the limit of metastability. The field h_{Spin} , corresponding to the instability, was extrapolated to the thermodynamic limit according to the finite-size scaling relation [19]

$$|h_{\text{Spin}} - h_L| \sim L^{-4/3}, \quad (17)$$

where h_L is the field at which the metastable phase becomes unstable for the given value of L .

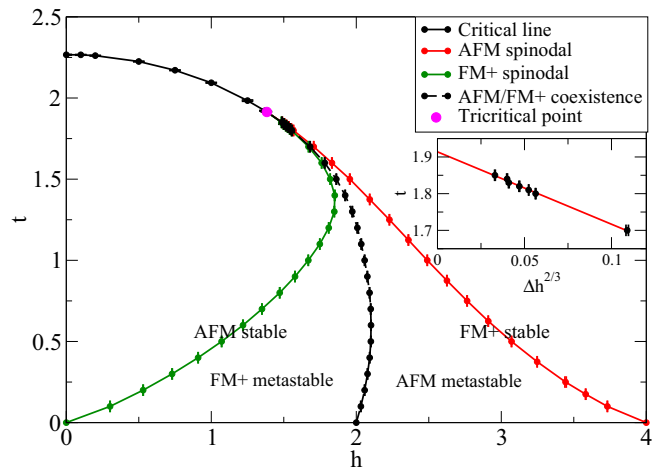


FIG. 4. (a) MC phase diagram for the full model with $a = 4$. Except for the absence of metastable FM phases at $h = 0$, the phase diagram resembles the mean-field phase diagram for $a = 7$, shown in Fig. 1. However, in contrast with the mean-field model, the line of critical points belongs to the two-dimensional Ising universality class. At $h = 0$ the critical temperature is near the exact Ising value, $t_c(h = 0) \approx 2.269$. Sharp spinodal lines extend from tricritical points at $t_3 \approx 1.914$ and $h_3 \approx \pm 1.383$, separated by a field distance in agreement with Eq. (15). The inset demonstrates this agreement near the tricritical point and was used to estimate its position. Δh is defined as in Fig. 1(a). See further discussion in the text.

A. $a = 4$

The h, t phase diagram for $a = 4$ is shown in Fig. 4. Except for the absence of metastable FM phases at $h = 0$, which is due to the lower value of a used here, the phase diagram is topologically identical to the mean-field phase diagram for $a = 7$, shown in Fig. 1. However, the line of critical points belongs to the Ising universality class, as evidenced by cumulant crossing values $U^* \approx 0.61$. At $h = 0$ the critical temperature is near the exact Ising value, $t_c(h = 0) = 2/\ln(1 + \sqrt{2}) \approx 2.269$, unaffected by the long-range interaction. Sharp spinodal lines extend from the tricritical point, separated by a field distance in agreement with Eq. (15) (see inset in Fig. 4). Near the tricritical point, values of L as large as 1024 were used. To estimate the position of the tricritical point, we extrapolated the separation between the L -extrapolated spinodal fields to zero according to Eq. (15) to find the tricritical temperature and from it the corresponding field values. The result is $t_3 \approx 1.914$ and $h_3 \approx \pm 1.383$. The coexistence line was obtained by the mixed start method with $L = 512$. No significant differences were observed with larger L .

We note that, for this relatively weak long-range interaction, our MC phase diagram shown in Fig. 4 is qualitatively similar to mean-field phase diagrams, both our Figs. 1 and 5 of Ref. [34]. However, for stronger long-range interactions, complex features that are not seen in the mean-field approximations are revealed by our MC simulations. These are discussed in Secs. IV B and IV C below.

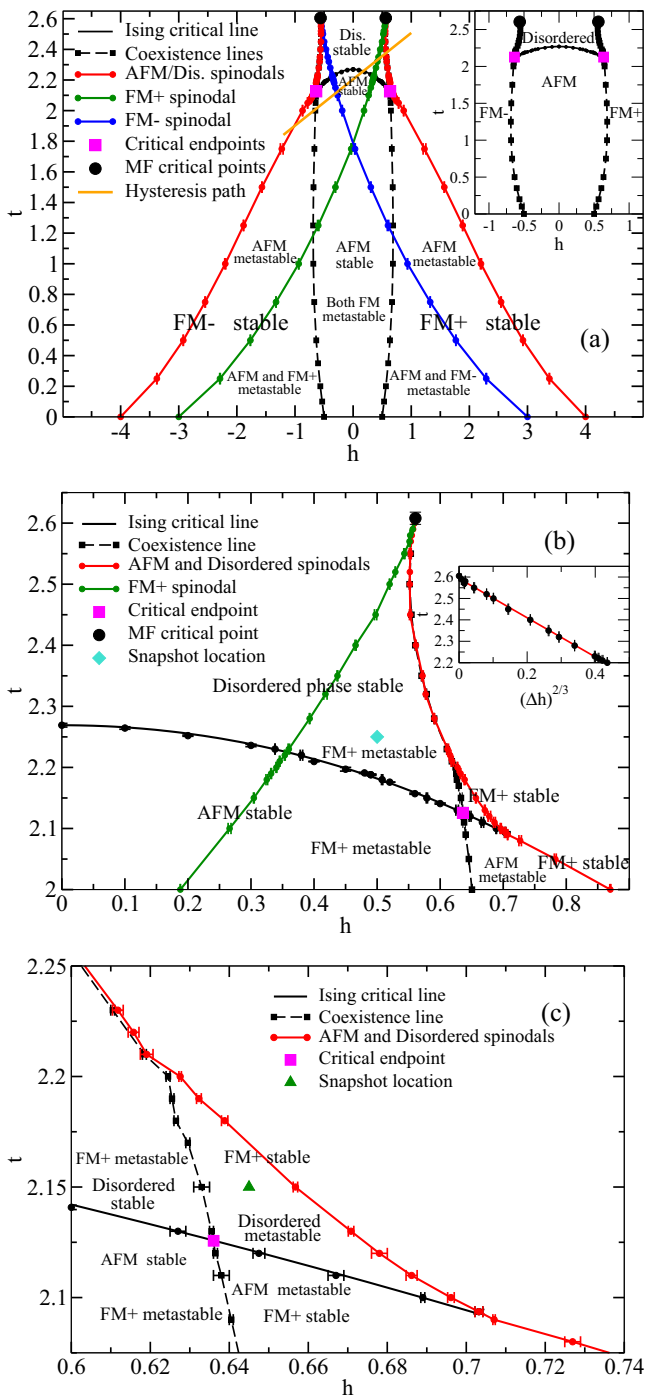


FIG. 5. (a) MC phase diagram in the h, t plane for the full model with $a = 7$. In contrast with the mean-field model [see Fig. 1(a)], the critical line is in the two-dimensional Ising universality class. Regions of phase stability and metastability are marked with text. The inset shows the phase diagram including only the stable phases. The diagonal line marks the path for the hysteresis loops in Fig. 7. (b) Detail of the horn region of the phase diagram. Our estimates of the positions of the critical end point and the mean-field critical points are $t = 2.126(1)$, $h = \pm 0.636(1)$ and $t = 2.61(1)$, $h = \pm 0.561(1)$, respectively. At $h = 0$ the critical temperature is near the exact Ising value. The diamond marks the position of the snapshots in Fig. 6. The inset demonstrates that the width of the horn region, Δh , obeys Eq. (15). The straight line is a guide to the eye. (c) Further magnified detail of the triangular region between the coexistence

B. $a = 7$

1. Phase diagram

The MC phase diagram in the h, t plane for $a = 7$ is shown in Fig. 5. Because of the stronger long-range interactions, metastable FM phases are possible for weak fields and low temperatures. However, the main difference from the case of $a = 4$ (Fig. 4) is that the tricritical points have been transformed into critical end points [60,61], where the line of Ising critical points meets the coexistence lines at a large angle (light gray squares, magenta online). Above the temperature of the critical end points, the coexistence lines continue toward higher temperatures, each eventually terminating at a mean-field critical point (large, black circles). Below the critical line and between the two coexistence lines, the stable phase is AFM. On the positive (negative) side of the right-hand (left-hand) coexistence line, the stable phase is FM+ (FM-). Above the critical line and between the coexistence lines, the stable phase is disordered with local fluctuations of AFM symmetry and a small magnetization in the direction of the applied field. For clarity, the inset in Fig. 5(a) shows the phase diagram with only the stable phases and corresponding phase transition lines and points included. The critical and coexistence lines were obtained as described above, with the coexistence lines calculated with $L = 1024$ to minimize the uncertainty. Our best estimates for the positions of the critical end points and mean-field critical points, based on simulations up to $L = 1024$ and finite-size scaling extrapolations, are $t = 2.126(1)$, $h = \pm 0.636(1)$ and $t = 2.61(1)$, $h = \pm 0.561(1)$, respectively. Since the full phase diagram, including metastable phase regions and spinodal lines is quite complicated, we present three, increasingly detailed views.

The main part of Fig. 5(a) shows the full range of temperatures and fields covered by the phase diagram, including the metastable phases and spinodal lines. The spinodal lines marking the limits of metastability of the FM+ and FM- phases cross the line of critical points at fields significantly weaker than those of the critical end points. Each of the FM spinodals continues on to meet the corresponding disorder spinodal at a mean-field critical point, forming a horn-like region of metastability. (As discussed below, the disorder spinodal and the disorder/FM coexistence line coincide within our numerical accuracy for $t \gtrsim 2.2$.) We located the critical point by scanning h at constant t across the coexistence line and monitoring the maximum of the susceptibility, χ_{\max} . At the critical point $\chi_{\max} \sim L^{\gamma/\nu_{\text{eff}}}$, with the mean-field exponents $\gamma = 1$ and $\nu_{\text{eff}} = 2/d = 1$ [6,62,63]. Above the critical temperature, the scaling is sublinear in L , and below it is superlinear. The gray (orange online), diagonal line corresponds to the path for the hysteresis loops shown in Fig. 7.

The main part of Fig. 5(b) shows a magnified image of the horn region. At this level of detail, two interesting phenomena become apparent. The first is that the Ising critical line (obtained from the crossings of fourth-order cumulants and

line, the critical line, and the spinodal line for the disordered phase. Here, the stable phase is FM+ (confirmed by simulations at the point marked with a triangle) and the disordered phase is metastable. See further discussion in the text.

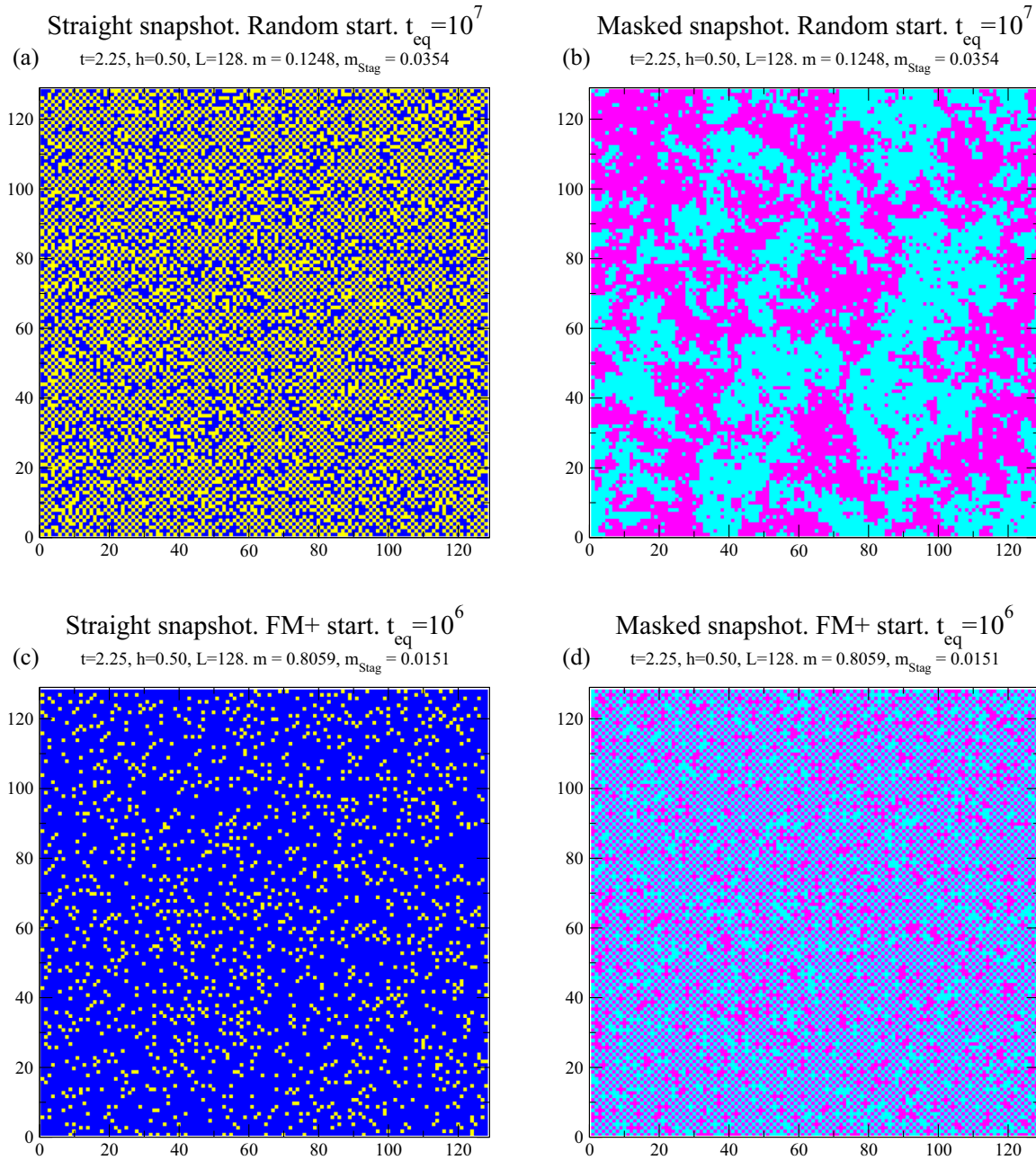


FIG. 6. Snapshots for $a = 7$ at $t = 2.25$ and $h = 0.50$ in the horn region [marked by a diamond in Fig. 5(b)]. (a) and (b) show the equilibrium disordered phase with AFM fluctuations. The system was initiated in an uncorrelated, random configuration and equilibrated for 10^7 MCSS before the image was recorded. (c) and (d) show the metastable FM+ phase. The system was initiated in the fully ordered FM+ configuration and “equilibrated” for 10^6 MCSS. In the “straight” images, (a) and (c), up and down spins are colored dark gray (blue online) and light gray (yellow online), respectively. The “masked” images (b) and (d) emphasize AFM domains by coloring up spins on the A sublattice dark gray (magenta online) and down on A, up on B light gray (cyan online).

linearly extrapolated to $1/L = 0$) continues beyond the critical end point where it meets the coexistence line, until it meets the spinodal line at $h \approx 0.705$. The triangular region limited by the coexistence line, the extended critical line, and the spinodal line is shown in further detail in Fig. 5(c). Our interpretation of this structure is that the extended critical line represents a nonequilibrium, second-order, Ising phase transition between a metastable AFM phase at lower temperatures and a metastable disordered phase inside the triangle. The existence of a true phase transition between two metastable phases is possible

because of the divergence of the metastable lifetimes in the thermodynamic limit. In this triangular region, FM+ has the lowest free energy and is therefore the stable phase. Conversely, in the rest of the horn region, the stable phase is the disordered phase, while FM+ is metastable. Snapshots of the stable and metastable phases in the latter region at the phase point marked by a diamond in Fig. 5(b) are shown in Fig. 6. (See methodological details in the caption of that figure.) In the triangular region in Fig. 5(c), the stability of FM+ was confirmed by starting systems with L up to 1024 with

a completely random spin configuration and equilibrating at $t = 2.15$ and $h = 0.645$ [marked by an up triangle in Fig. 5(c)] for 10^7 MCSS before measuring the order parameters. The metastability of the disordered phase in the same region was confirmed by scanning h in the positive direction across the coexistence line until it decayed discontinuously to FM+ at the spinodal. At the point where the extended critical line meets the spinodal line, the interpretation of the latter changes from the limit of metastability of the AFM phase at lower t to being the limit of metastability of the disordered phase at higher t . The line was determined by the same method in both temperature regions.

The second phenomenon observed in Figs. 5(b) and 5(c) is that, above $t \approx 2.20$, the coexistence line and the spinodal line for the disordered phase coincide within our numerical accuracy. The inset in Fig. 5(b) demonstrates that the separation of the spinodals near the tip of each horn obeys Eq. (15). At $h = 0$ the critical temperature is again near the exact Ising value, $t_c(h = 0) \approx 2.269$, unaffected by the long-range interaction.

2. Hysteresis loops

The phase diagram for $a = 7$, shown in Fig. 5, suggests the existence of complex hysteresis loops. Constant-temperature hysteresis loops for two different temperatures in the horn region are shown in Fig. 7. In Fig. 7(a) we use $t = 2.18$, which lies between the temperature of the critical end point and the temperature at which the FM spinodal lines cross the critical line. Following the curves in the negative direction from $h = +0.8$, the system starts in the stable FM+ phase, which becomes metastable as the phase point crosses the coexistence line at $h \approx +0.63$. [Note that the disorder/FM coexistence lines are at only slightly weaker fields than the disorder spinodal lines at this temperature. See Figs. 5(b) and (c).] Crossing the FM+ spinodal line at $h \approx +0.33$, the system changes discontinuously to the equilibrium AFM phase. It remains in this phase until it crosses the critical line into the equilibrium disordered phase at $h \approx -0.52$. Finally there is a discontinuous change to the FM- phase across the disorder spinodal at $h \approx -0.63$. The sequence is symmetric in h as the field is reversed from $h = -0.8$ back to $+0.8$.

Raising the temperature to $t = 2.25$ (which lies between the temperature at which the FM spinodals cross the critical line and the zero-field critical temperature) in Fig. 7(b), the main difference is that the system changes discontinuously from the FM+ phase to the equilibrium disordered phase at $h \approx +0.38$, only passing into the equilibrium AFM phase as it crosses the critical line at $h \approx +0.24$. At $h \approx -0.24$ it again crosses the critical line into the disordered phase, which it leaves through a discontinuous jump as it crosses out of the horn region at the negative disorder spinodal at $h \approx -0.60$. The path is again symmetric during the field reversal. At both temperatures the nonzero values of the staggered magnetization in the disordered equilibrium phase are a finite-size effect.

When using the model studied here to represent phase transitions in SC materials, the magnetic field is replaced by the temperature-dependent effective field of Eq. (2). A path for temperature driven hysteresis within this interpretation of the model is represented by the diagonal line segment in Fig. 5(a)

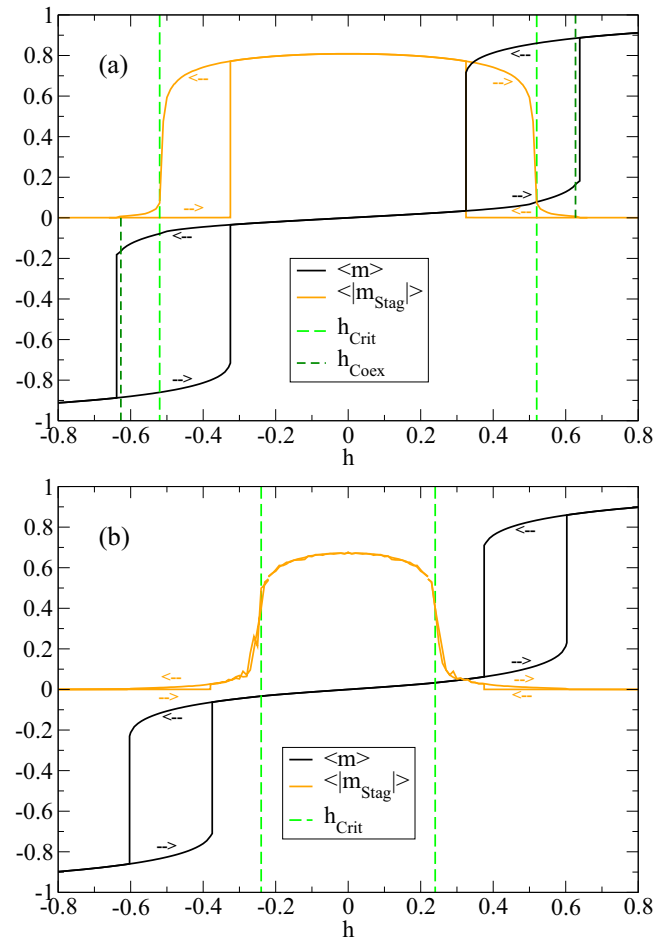


FIG. 7. Constant-temperature hysteresis loops for $a = 7$. The system size was $L = 512$, except near where the hysteresis path crosses the critical line [marked with light gray (green online) vertical, dashed lines] and in the disordered phase, where $L = 1024$ was used. The nonzero values of m_{Stag} in the disordered phase are a finite-size effect. (a) At $t = 2.18$. The metastable FM+ phase decays discontinuously into the ordered AFM phase at the FM+ spinodal near $h = +0.34$. The loops are symmetric under reversal of h and m . The dark, vertical, short-dashed lines mark the coexistence lines between the disordered and FM phases. At this temperature they lie very close to the disorder spinodals. (b) At $t = 2.25$. The metastable FM+ phase decays discontinuously into the disordered phase at the FM+ spinodal near $h = +0.39$. The loops are symmetric under reversal of h and m . At this temperature, the disorder/FM coexistence lines and the disorder spinodals coincide within our numerical accuracy. See further discussion in the text.

(degeneracy ratio $\ln g = 20/3$ and energy difference $D = 18|J|$). The corresponding phase transitions and hysteresis loops are shown in Fig. 8. The loops are asymmetric. The narrow loop above the critical temperature corresponds to passage across the positive- h horn, while the wider loop below the critical temperature lies between the negative AFM spinodal and the FM- spinodal. The nonzero values of m_{Stag} in the disordered phase region are again a finite-size effect.

We note that the pattern of transitions and hysteresis loops shown in Fig. 8 closely resembles recent experimental results for thermal two-step transitions with hysteresis in several

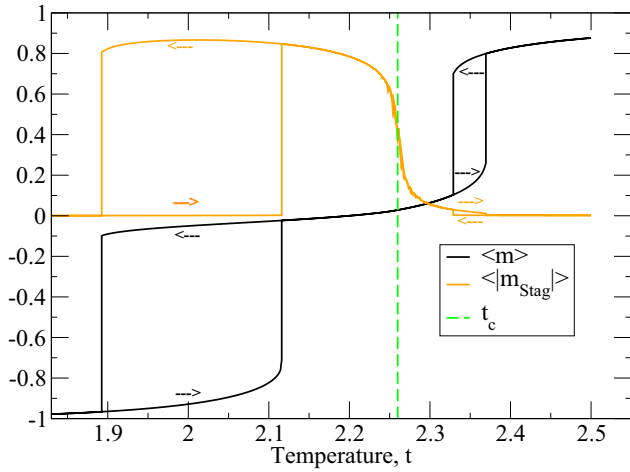


FIG. 8. Asymmetric thermal hysteresis loops for $a = 7$ along the path marked by a diagonal line segment in Fig. 5(a). The vertical, dashed line marks the temperature where the path crosses the line of AFM Ising critical points. Simulated with $L = 256$. The nonzero values of m_{Stag} in the disordered phase are a finite-size effect. This pattern of transitions and hysteresis loops closely resembles recent experimental results for thermal two-step transitions with hysteresis in several different SC materials [35–40]. See further discussion in the text.

different SC materials [35–40]. Some of these experiments are also discussed in two recent reviews of this rapidly developing field [64,65].

C. $a = 10$

For $a > 8$ there is no stable AFM phase. The h, t phase diagram with $a = 10$ is shown for $h \geq 0$ in Fig. 9(a). The phase diagram is symmetric around $h = 0$. The black curve with data points in the main figure shows the FM– spinodal. For weak fields and temperatures below the Ising critical temperature [$t_c(h = 0) \approx 2.269$], there also exists a metastable AFM phase. It is separated from the stable FM phases by sharp mean-field spinodals. At higher temperatures, this AFM phase undergoes a second-order transition to a metastable disordered phase. These metastable phases are separated by a line of critical points in the Ising universality class. (Located and identified by the fourth-order cumulant method as above.) At $h = 0$, the disordered phase is metastable between the zero-field Ising critical temperature and $t \approx 2.68$. Like the metastable AFM phase, it is separated from the equilibrium FM phases by sharp mean-field spinodals. A magnified view of the region containing the metastable disordered phase is shown in the inset in Fig. 9(a). The spinodals and the metastable critical line shown in Fig. 9(a) were obtained from finite-size scaling extrapolations of MC data up to $L = 1024$. These features do not appear in the simple mean-field approximation shown in Fig. 3(a). Stable and metastable order parameters at $h = 0$ are shown in Fig. 9(b), corresponding to the mean-field results shown in Fig. 3(b). The MC simulations for the metastable order parameter are seen to be in excellent agreement with the Onsager-Yang exact order parameter for a square-lattice Ising model in zero field [66], $m_{\text{Stag}}(t, 0) = \{1 - [\sinh(2/t)^{-4}]\}^{1/8}$. The metastable disordered phase is characterized by values

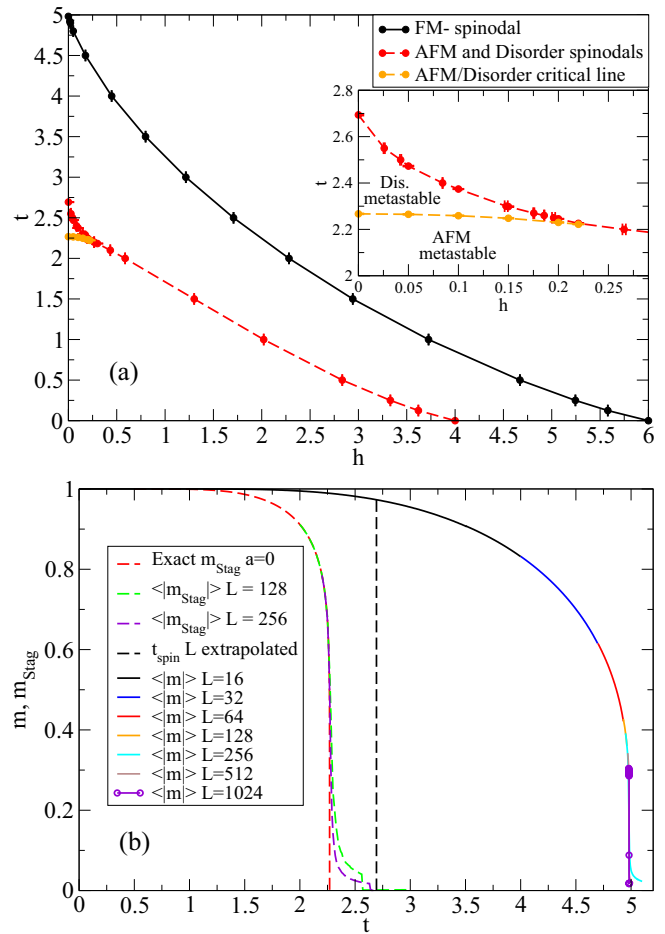


FIG. 9. (a) h, t phase diagram for $a = 10$. The FM+ phase is stable everywhere in this figure, and FM– is metastable everywhere below the black spinodal curve. The AFM phase is metastable below the medium gray (red online) spinodal and light gray (orange online) critical curves, and the disordered phase is metastable inside the triangle between these curves. The inset shows an enlarged view of the region around the metastable disordered phase. The phase diagram is symmetric under simultaneous sign change of h and exchange of the FM+ and FM– phases. (b) Stable FM order parameter m (solid curves) and metastable AFM order parameter m_{Stag} (dashed curves), shown vs t at $h = 0$. The FM order parameter is shown for a composite of system sizes, $L = 16, \dots, 1024$, identified online by different colors. The data for $L = 512$ and 1024 indicate that the transition is weakly first order. The AFM order parameter is shown as the exact, Onsager order parameter and MC simulations for $L = 128$ and 256 . The metastable disordered phase lies between the Ising critical temperature and the L -extrapolated spinodal temperature marked by the vertical, dashed line. See further discussion in the text.

of the simulated m_{Stag} that decrease linearly with L and go discontinuously to zero at a sharp spinodal temperature. This phase lies between the Ising critical temperature and the spinodal temperature, whose L -extrapolated value is marked by a vertical, dashed line. If the system is heated in the metastable phases, this is the temperature at which the stable order parameter m will jump discontinuously from near zero to its equilibrium value. The observation of a critical line separating the metastable AFM and disordered phases in this

large- a regime supports our interpretation of the critical line in the small part of the horn region for $a = 7$, shown in Fig. 5(c) as a transition line separating two metastable phases.

The phase transition of the stable FM phase at $t \approx 4.98$ involves a small discontinuity (seen only for $L = 1024$) and negative values of the Binder cumulants above the transition temperature (seen for $L = 1024$ and 512, not shown). These features suggest that this transition is weakly first order. Exploratory simulations for $a = 8.5$ and $a = 20$ at $h = 0$ indicate a strongly first-order transition in the former case, and a continuous transition in the mean-field universality class in the latter. Further investigation of the strong long-range interaction regime of $a \geq 8$ is left for future study.

V. CONCLUSIONS

In this paper we present a detailed investigation of the phase diagrams of a simplified model of an SC material with a two-step transition as a square-lattice Ising model with AFM nearest-neighbor interactions and FM long-range interactions of the Husimi-Temperley (equivalent-neighbor) kind. An AFM equilibrium phase for weak applied fields is replaced by field-induced FM phases at stronger fields. These phases are separated by coexistence lines surrounded by sharp spinodal lines representing limits of metastability.

In a range of intermediate-strength long-range interactions, we find significant differences between the phase diagrams of this model, calculated by importance-sampling MC simulations, and those of a model in which fluctuations have been neglected by replacing the nearest-neighbor interactions by a two-sublattice mean-field approximation. The difference consists in the replacement of each tricritical point in the

mean-field model with a pair consisting of a critical end point and a mean-field critical point in the h, t phase diagram, surrounded by horns representing metastable phases. For even stronger long-range interactions, the AFM equilibrium phase disappears. However, metastable AFM and disordered phases can still be observed. These complex phase diagrams give rise to hysteresis loops reminiscent of two-step transitions observed in several SC materials [26–42,64,65].

We find it likely that the horn type phase diagrams and related two-step hysteresis loops revealed in our model by MC simulations may be observed in more realistic models of SC materials with elastic interactions [24], and also in future experiments. An investigation into the former possibility is in progress [67]. Other interesting avenues of further research include cluster mean-field approximations for the short-range AFM interactions [52] and calculation of free-energy surfaces in the m_A, m_B plane by Wang-Landau MC simulations [68].

ACKNOWLEDGMENTS

P.A.R. and C.O. gratefully acknowledge hospitality by the Department of Physics, University of Tokyo. P.A.R. thanks H.R.D. Barclay for useful suggestions. Work at Florida State University was supported in part by U.S. NSF Grant No. DMR-1104829. G.B. is supported by Oak Ridge National Laboratory, which is managed by UT-Battelle, LLC. The work was also supported by Grants-in-Aid for Scientific Research C (No. 26400324 and No. 25400391) from MEXT of Japan, and the Elements Strategy Initiative Center for Magnetic Materials under the outsourcing project of MEXT. The numerical calculations were supported by the supercomputer center of ISSP of The University of Tokyo and the Florida State University Research Computing Center.

-
- [1] C. Teodosiu, *Elastic Models of Crystal Defects* (Springer-Verlag, Berlin, 1982), Chap. 5.
 - [2] X. Zhu, F. Tavazza, D. P. Landau, and B. Dünweg, Critical behavior of an elastic Ising antiferromagnet at constant pressure, *Phys. Rev. B* **72**, 104102 (2005).
 - [3] W. Klein, H. Gould, N. Gulbache, J. B. Rundle, and K. Tiampo, Structure of fluctuations near mean-field critical points and spinodals and its implication for physical processes, *Phys. Rev. E* **75**, 031114 (2007).
 - [4] K. Binder, Nucleation barriers, spinodal, and the Ginzburg criterion, *Phys. Rev. A* **29**, 341 (1984).
 - [5] S. Miyashita, Y. Konishi, M. Nishino, H. Tokoro, and P. A. Rikvold, Realization of the mean-field universality class in spin-crossover materials, *Phys. Rev. B* **77**, 014105 (2008).
 - [6] T. Nakada, P. A. Rikvold, T. Mori, and S. Miyashita, Crossover between a short-range and a long-range Ising model, *Phys. Rev. B* **84**, 054433 (2011).
 - [7] T. Nakada, T. Mori, S. Miyashita, M. Nishino, S. Todo, W. Nicolazzi, and P. A. Rikvold, Critical temperature and correlation length of an elastic interaction model for spin-crossover materials, *Phys. Rev. B* **85**, 054408 (2012).
 - [8] C. Enachescu, R. Tanasa, A. Stancu, F. Varret, J. Linares, and E. Codjovi, First-order reversal curves analysis of rate-dependent hysteresis: The example of light-induced thermal hysteresis in a spin-crossover solid, *Phys. Rev. B* **72**, 054413 (2005).
 - [9] M. Nishino, K. Boukheddaden, Y. Konishi, and S. Miyashita, Simple Two-dimensional Model for the Elastic Origin of Cooperativity Among Spin States of Spin-crossover Complexes, *Phys. Rev. Lett.* **98**, 247203 (2007).
 - [10] Y. Konishi, H. Tokoro, M. Nishino, and S. Miyashita, Monte Carlo Simulation of Pressure-induced Phase Transitions in Spin-crossover Materials, *Phys. Rev. Lett.* **100**, 067206 (2008).
 - [11] A. Bousseksou, G. Molnár, L. Salmon, and W. Nicolazzi, Molecular spin crossover phenomenon: Recent achievements and prospects, *Chem. Soc. Rev.* **40**, 3313 (2011).
 - [12] *Spin-crossover Materials—Properties and Applications*, edited by M. A. Halcrow (John Wiley & Sons, Chichester, UK, 2013).
 - [13] P. Gütllich, A. Hauser, and H. Spiering, Thermal and optical switching of iron(II) complexes, *Ang. Chem., Int. Ed. Eng.* **33**, 2024 (1994).
 - [14] C. Chong, F. Varret, and K. Boukheddaden, Evolution of self-organized spin domains under light in single-crystalline $[\text{Fe}(\text{ptz})_6](\text{BF}_4)_2$, *Phys. Rev. B* **81**, 014104 (2010).
 - [15] S. Ohkoshi, K. Imoto, Y. Tsunobuchi, S. Takano, and H. Tokoro, Light-induced spin-crossover magnet, *Nat. Chem.* **3**, 564 (2011).
 - [16] A. Asahara, M. Nakajima, R. Fukaya, H. Tokoro, S. Ohkoshi, and T. Suemoto, Growth dynamics of photoinduced phase

- domain in cyano-complex studied by boundary sensitive Raman spectroscopy, *Acta Phys. Pol. A* **121**, 375 (2012).
- [17] P. Chakraborty, C. Enachescu, A. Humair, L. Egger, T. Delgado, A. Tissot, L. Guenee, C. Besnard, R. Bronisz, and A. Hauser, Light-induced spin-state switching in the mixed crystal series of the 2d coordination network $\{[Zn_{1-x}Fe_x(bbtr)_3](BF_4)_2\}_\infty$: Optical spectroscopy and cooperative effects, *Dalton Trans.* **43**, 17786 (2014).
- [18] S. Miyashita, Y. Konishi, H. Tokoro, M. Nishino, K. Boukheddaden, and F. Varret, Structures of metastable states in phase transitions with a high-spin low-spin degree of freedom, *Prog. Theor. Phys.* **114**, 719 (2005).
- [19] S. Miyashita, P. A. Rikvold, T. Mori, Y. Konishi, M. Nishino, and H. Tokoro, Threshold phenomena under photoexcitation of spin-crossover materials with cooperativity due to elastic interactions, *Phys. Rev. B* **80**, 064414 (2009).
- [20] O. Kahn and C. Jay Martinez, Spin-transition polymers: From molecular materials toward memory devices, *Science* **279**, 44 (1998).
- [21] J. Linares, E. Codjovi, and Y. Garcia, Pressure and temperature spin crossover sensors with optical detection, *Sensors* **12**, 4479 (2012).
- [22] H. Spiering, K. Boukheddaden, J. Linares, and F. Varret, Total free energy of a spin-crossover molecular system, *Phys. Rev. B* **70**, 184106 (2004).
- [23] J. Wajnlasz and R. Pick, Transitions “low spin”–“high spin” dans les complexes de Fe^{2+} , *J. Phys. (Paris), Colloq.* **32**, C1-91 (1971).
- [24] M. Nishino and S. Miyashita, Effect of the short-range interaction on critical phenomena in elastic interaction systems, *Phys. Rev. B* **88**, 014108 (2013).
- [25] T. Mori, S. Miyashita, and P. A. Rikvold, Asymptotic forms and scaling properties of the relaxation time near threshold points in spinodal type dynamical phase transitions, *Phys. Rev. E* **81**, 011135 (2010).
- [26] H. Köppen, E. W. Müller, C. P. Köhler, H. Spiering, E. Meissner, and P. Gütllich, Unusual spin-transition anomaly in the crossover system $[Fe(2-pic)_3]Cl_2 \cdot EtOH$, *Chem. Phys. Lett.* **91**, 348 (1982).
- [27] V. V. Zelentsov, G. I. Lapouchkine, S. S. Sobolev, and V. I. Shipilov, Model for two-stage spin transitions, *Dokl. Akad. Nauk* **289**, 393 (1985).
- [28] V. Petrouleas and J.-P. Tuchagues, $Fe[5NO_2-sal-N(1,4,7,10)]$: A new iron(II) complex exhibiting an unusual two-step spin conversion afforded by a hexadentate ligand with a N_4O_2 donor set, *Chem. Phys. Lett.* **137**, 21 (1987).
- [29] A. Bousseksou, J. Nasser, J. Linares, K. Boukheddaden, and F. Varret, Ising-like model for the two-step spin-crossover, *J. Phys. I (France)* **2**, 1381 (1992).
- [30] R. Jakobi, H. Spiering, and P. Gütllich, Thermodynamics of the spin transition in $[Fe_xZn_{1-x}(2-pic)_3]Cl_2 \cdot EtOH$, *J. Phys. Chem. Solids* **53**, 267 (1992).
- [31] J. A. Real, H. Bolvin, A. Bousseksou, A. Dworkin, O. Kahn, F. Varret, and J. Zarembowitch, Two-step spin crossover in the new dinuclear compound $[Fe(bt)(NCS)_2]_2bpym$, with $bt = 2,2'$ -bi-2-thiazoline and $bpym = 2,2'$ -bipyrimidine: Experimental investigation and theoretical approach, *J. Am. Chem. Soc.* **114**, 4650 (1992).
- [32] D. Boinnard, A. Bousseksou, A. Dworkin, J. M. Savariault, F. Varret, and J. P. Tuchagues, Two-step spin conversion of $[Fe^{II}(5-NO_2-sal-N(1,4,7,10))]$: 292, 153, and 103 K x-ray crystal and molecular structure, infrared, magnetic, Mössbauer, calorimetric, and theoretical studies, *Inorg. Chem.* **33**, 271 (1994).
- [33] H. Bolvin, The Neel point for spin-transition systems: Toward a two-step transition, *Chem. Phys.* **211**, 101 (1996).
- [34] D. Chernyshov, H.-B. Bürgi, M. Hostettler, and K. W. Törnroos, Landau theory for spin transition and ordering phenomena in Fe(II) compounds, *Phys. Rev. B* **70**, 094116 (2004).
- [35] S. Bonnet, M. A. Siegler, J. S. Costa, G. Molnár, A. Bousseksou, A. L. Spek, P. Gamez, and J. Reedijk, A two-step spin crossover mononuclear iron(II) complex with a [HS-LS-LS] intermediate phase, *Chem. Commun.* **43**, 5619 (2008).
- [36] S. Pillet, E.-E. Bendeif, S. Bonnet, H. J. Shepherd, and P. Guionneau, Multimetastability, phototrapping, and thermal trapping of a metastable commensurate superstructure in a Fe^{II} spin-crossover compound, *Phys. Rev. B* **86**, 064106 (2012).
- [37] M. Buron-Le Cointe, N. Ould Moussa, E. A. Trzop, A. Moréac, G. Molnár, L. Toupet, A. Bousseksou, J. F. Létard, and G. S. Matouzenko, Symmetry breaking and light-induced spin-state trapping in a mononuclear Fe^{II} complex with the two-step thermal conversion, *Phys. Rev. B* **82**, 214106 (2010).
- [38] J.-B. Lin, W. Xue, B.-Y. Wang, J. Tao, W.-X. Zhang, J.-P. Zhang, and X.-M. Chen, Chemical/physical pressure tunable spin-transition temperature and hysteresis in a two-step spin crossover porous coordination framework, *Inorg. Chem.* **51**, 9423 (2012).
- [39] Y. M. Klein, N. F. Sciortino, F. Ragon, C. E. Housecroft, C. J. Kepert, and S. M. Neville, Spin crossover intermediate plateau stabilization in a flexible 2-D Hofmann-type coordination polymer, *Chem. Commun.* **50**, 3838 (2014).
- [40] D. J. Harding, W. Phonsri, P. Harding, K. S. Murray, B. Moubaraki, and G. N. L. Jameson, Abrupt two-step and symmetry breaking spin crossover in an iron(III) complex: an exceptionally wide [LS–HS] plateau, *Dalton Trans.* **44**, 15079 (2015).
- [41] D. Chernyshov, M. Hostettler, K. W. Törnroos, and H.-B. Bürgi, Ordering phenomena and phase transitions in a spin-crossover compound – uncovering the nature of the intermediate phase of $[Fe(2-pic)_3]Cl_2EtOH$, *Ang. Chem. Int. Ed.* **42**, 3825 (2003).
- [42] N. Huby, L. Guérin, E. Collet, L. Toupet, J.-C. Ameline, H. Cailleau, and T. Roisnel, Photoinduced spin transition probed by x-ray diffraction, *Phys. Rev. B* **69**, 020101(R) (2004).
- [43] G. Brown, P. A. Rikvold, and S. Miyashita, Monte Carlo studies of the Ising antiferromagnet with a ferromagnetic mean-field term, *Phys. Proc.* **57**, 20 (2014).
- [44] E. Jordão Neves and R. H. Schonmann, Critical droplets and metastability for a Glauber dynamics at very low-temperatures, *Commun. Math. Phys.* **137**, 209 (1991).
- [45] W. L. Bragg and E. J. Williams, The effect of thermal agitation on atomic arrangement in alloys, *Proc. R. Soc. A* **145**, 699 (1934).
- [46] W. L. Bragg and E. J. Williams, The effect of thermal agitation on atomic arrangement in alloys–II, *Proc. R. Soc. A* **151**, 540 (1935).

- [47] R. Osorio, Generalized Bragg-Williams method for antiferromagnetic lattice gases, *Rev. Bras. Fís.* **13**, 515 (1983).
- [48] D. P. Landau, Magnetic Tricritical Points in Ising Antiferromagnets, *Phys. Rev. Lett.* **28**, 449 (1972).
- [49] D. P. Landau and R. H. Swendsen, Tricritical Universality in Two Dimensions, *Phys. Rev. Lett.* **46**, 1437 (1981).
- [50] P. A. Rikvold, W. Kinzel, J. D. Gunton, and K. Kaski, Finite-size scaling study of a two-dimensional lattice-gas model with a tricritical point, *Phys. Rev. B* **28**, 2686 (1983).
- [51] C. M. Newman and L. S. Schulman, Complex free-energies and metastable lifetimes, *J. Stat. Phys.* **23**, 131 (1980).
- [52] Better agreement between mean-field and MC results can be obtained by including some fluctuation effects through cluster mean-field approximations with clusters of at least 6×6 spins [53]. However, this approach will not change the universality class of critical lines.
- [53] C. Omand, S. Miyashita, and P. A. Rikvold (unpublished).
- [54] K. Binder, Critical Properties From Monte Carlo Coarse Graining and Renormalization, *Phys. Rev. Lett.* **47**, 693 (1981).
- [55] G. Kamieniarz and H. Blöte, Universal ratio of magnetization moments in two-dimensional Ising models, *J. Phys. A: Math. Gen.* **26**, 201 (1993).
- [56] X. S. Chen and V. Dohm, Nonuniversal finite-size scaling in anisotropic systems, *Phys. Rev. E* **70**, 056136 (2004).
- [57] W. Selke and L. N. Shchur, Critical Binder cumulant in two-dimensional anisotropic Ising models, *J. Phys. A: Math. Gen.* **38**, L739 (2005).
- [58] H. Tomita, A. Ito, and H. Kidachi, Eigenvalue problem of metastability in macrosystem, *Prog. Theor. Phys.* **56**, 786 (1976).
- [59] P. A. Rikvold, H. Tomita, S. Miyashita, and S. W. Sides, Metastable lifetimes in a kinetic Ising model: Dependence on field and system size, *Phys. Rev. E* **49**, 5080 (1994).
- [60] B. Widom, Noncritical interface near a critical end point, *J. Chem. Phys.* **67**, 872 (1977).
- [61] J. B. Collins, P. A. Rikvold, and E. T. Gawlinski, Finite-size scaling analysis of the $S = 1$ Ising model on the triangular lattice, *Phys. Rev. B* **38**, 6741 (1988).
- [62] V. Privman and M. E. Fisher, Finite-size effects at first-order transitions, *J. Stat. Phys.* **33**, 385 (1983).
- [63] E. Luijten and H.-W.-J. Blöte, Classical critical behavior of spin models with long-range interactions, *Phys. Rev. B* **56**, 8945 (1997), and references cited therein.
- [64] M. Shatruk, H. Phan, B. A. Chrisostomo, and A. Suleimенова, Symmetry-breaking structural phase transitions in spin crossover complexes, *Coord. Chem. Rev.* **289-290**, 62 (2015).
- [65] S. Brooker, Spin crossover with thermal hysteresis: Practicalities and lessons learnt, *Chem. Soc. Rev.* **44**, 2880 (2015).
- [66] R. K. Pathria and P. D. Beale, *Statistical Mechanics, Third Edition* (Butterworth-Heinemann, Oxford, 2011), Chap. 13, and references cited therein.
- [67] M. Nishino, S. Miyashita, and P. A. Rikvold (unpublished).
- [68] C. H. Chan, G. Brown, P. A. Rikvold, and S. Miyashita (unpublished).